

# Simulation of Electron Cloud Effects in the PETRA Positron Storage Ring

R. Wanzenberg

DESY, Notkestr. 85, 22603 Hamburg, Germany

December 10, 2003

## **Abstract**

In positron storage rings electrons produced by photoemission, ionization and secondary emission accumulate in the vacuum chamber and form an "electron cloud" which can reach a high charge density for some beam operation modes. Electron cloud effects have not been observed in the present operation mode of the PETRA II ring used as a preaccelerator for HERA, but with the high performance goals of the planned synchrotron radiation facility PETRA III a more complete understanding of electron cloud development and its effects on the positron beam are needed to aid in the design. The computer code E-CLOUD 2.3 is used to simulate electron cloud effects for different operation modes of PETRA II and PETRA III. An effective transverse single bunch wakefield due to the electron cloud is obtained from a broad band resonator model.

# Contents

|          |   |           |
|----------|---|-----------|
| <b>1</b> | <b>Introduction</b>   | <b>3</b>  |
| <b>2</b> | <b>PETRA II and PETRA III parameters</b>                    | <b>5</b>  |
| 2.1      | Beam parameters and beam optics . . . . .                   | 5         |
| 2.1.1    | Beam parameters . . . . .                                   | 5         |
| 2.1.2    | PETRA III beam optics . . . . .                             | 6         |
| 2.2      | The vacuum chamber . . . . .                                | 8         |
| 2.3      | Photoelectrons and secondary emission . . . . .             | 11        |
| 2.3.1    | Photoelectrons . . . . .                                    | 11        |
| 2.3.2    | Secondary emission . . . . .                                | 14        |
| <b>3</b> | <b>Simulation of the electron cloud build-up</b>            | <b>18</b> |
| 3.1      | PETRA II . . . . .  | 18        |
| 3.1.1    | PETRA II – Standard fill with 96 ns bunch spacing . . . . . | 18        |
| 3.1.2    | PETRA II – Special fill with 10 ns bunch spacing . . . . .  | 20        |
| 3.2      | PETRA III . . . . .   | 21        |
| 3.2.1    | PETRA III – Variant A . . . . .                             | 22        |
| 3.2.2    | PETRA III – Variant B . . . . .                             | 25        |
| 3.2.3    | Summary of the PETRA simulation results . . . . .           | 25        |
| 3.3      | KEK-B LER . . . . .   | 28        |
| <b>4</b> | <b>Single bunch instabilities due to electron clouds</b>    | <b>31</b> |
| 4.1      | Broad band resonator model . . . . .                        | 31        |
| 4.2      | Estimates for the instability thresholds . . . . .          | 32        |
| 4.3      | Wakefields due to electron clouds . . . . .                 | 34        |
| <b>5</b> | <b>Summary and conclusion</b>                               | <b>35</b> |
|          | <b>References</b>   | <b>37</b> |

# 1 Introduction

The PETRA ring is presently used as a preaccelerator for the HERA lepton hadron collider ring at DESY. Positron currents of about 50 mA are injected at an energy of 7 GeV and accelerated to the HERA injection energy of 12 GeV. It is planned to rebuild the PETRA ring into a synchrotron radiation facility [1], called PETRA III, after the end of the present HERA collider physics program. One section of the PETRA ring will be completely redesigned to provide space for several undulators. The planned facility aims for a very high brilliance of about  $10^{21}$  photons/s/0.1%BW/mm<sup>2</sup>/mrad<sup>2</sup> using a low emittance (1 nm rad) positron beam with an energy of 6 GeV. The planned location for the new hall is shown in Fig. 1. A more detailed layout of the hall and the synchrotron radiation beam lines is shown in Fig. 2

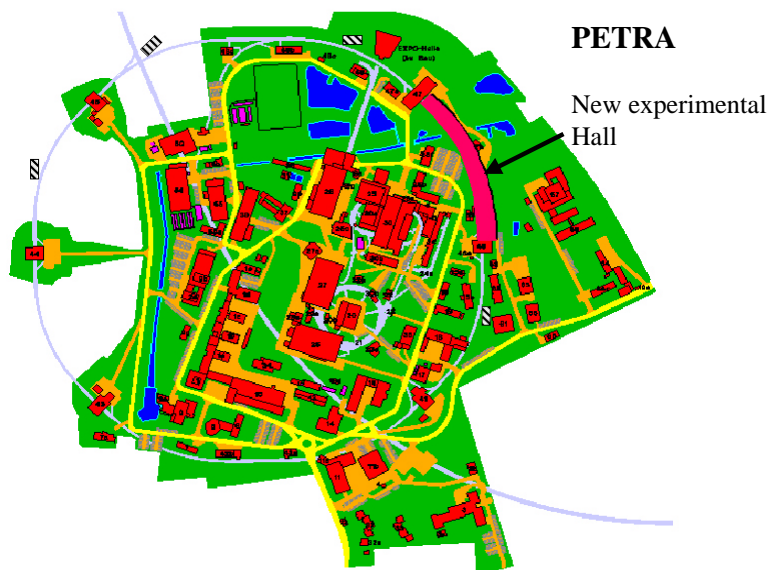


Figure 1: Ground plan of the DESY site with the PETRA ring. The location of the planned new experimental hall is also shown.

In positron storage rings electrons produced by photoemission, ionization and secondary emission accumulate in the vacuum chamber forming an "electron cloud" with a charge density which depends on the beam operation mode. For certain modes with short bunch spacings and high intensities a high cloud density disturbs the beam. Experimental observations of effects due to electron clouds have been reported from existing accelerators operating with high beam current like the B-factories (KEKB, PEP-II) [2, 3]. In 1995, a multi-bunch instability, seen at the KEK photon factory since the start of the positron beam operation in 1989, was explained by bunch-to-bunch coupling via electron clouds [5, 4]. Earlier observations of electron clouds, dating back to 1966 and 1977, have been reported from proton storage rings [6, 7]. The present understanding of

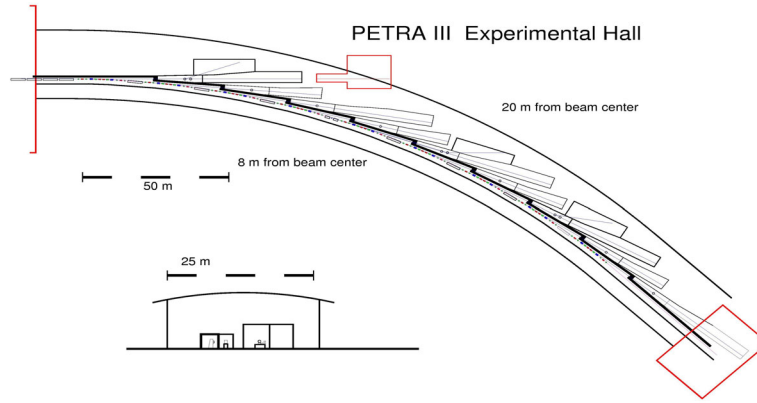


Figure 2: Layout of the new experimental hall for synchrotron radiation experiments.

the build-up of an electron cloud and of the effects of the cloud on the positron beam are based on computer simulations and measurements with different types of detectors. A summary is given in [8, 9, 10, 11].

Electron cloud effects have not been observed in the present operation mode of the PETRA accelerator as a preaccelerator for HERA (referred to as PETRA II) with moderate bunch currents and relatively large bunch spacings, but with the high performance goals of the planned facility PETRA III a more complete understanding of electron cloud development and its effects on the positron beam are needed to aid in the design. The computer code E-CLOUD 2.3 by F. Zimmermann et al. [12] is used to simulate electron cloud effects for different operation modes of PETRA II and PETRA III. An example from an electron cloud simulation for PETRA II is shown in Fig. 3. The operation parameters used for the simulations are discussed in the next section while the simulation results are presented in section 3.

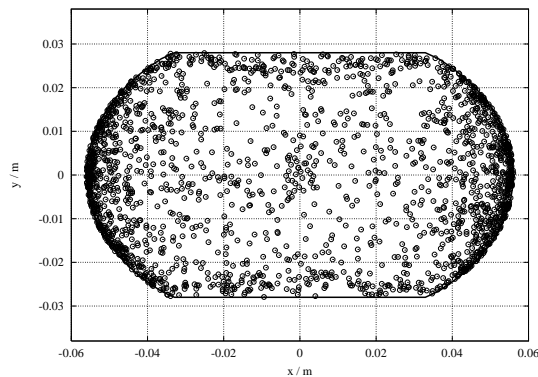


Figure 3: Simulation of an electron cloud in the PETRA II vacuum chamber using E-CLOUD 2.3.

## 2 PETRA II and PETRA III parameters

For the simulation of the build-up of an electron cloud it is important to know the beam parameters, the vacuum chamber geometry and the secondary electron emission yield of the vacuum chamber material. The data for the PETRA II and the planned PETRA III positron storage rings are summarized in this section.

### 2.1 Beam parameters and beam optics

#### 2.1.1 Beam parameters

Four sets of beam parameters are considered for the electron cloud simulations: PETRA II with 96 ns and 10 ns bunch spacing and two operation modes of the planned synchrotron facility PETRA III. The parameters are summarized in Tab. 1. The PETRA II parameters with 96 ns bunch spacing are typical

|                                      | PETRA II |         | PETRA III |         |
|--------------------------------------|----------|---------|-----------|---------|
|                                      | 96 ns    | 10 ns   | A         | B       |
| Energy /GeV                          | 7        | 7       | 6         | 6       |
| Circumference /m                     | 2304.0   | 2304.0  | 2304.0    | 2304.0  |
| Bending radius /m                    | 191.729  | 191.729 | 191.729   | 191.729 |
| Revolution frequency /kHz            | 130.1    | 130.1   | 130.1     | 130.1   |
| Bunch Population / $10^{10}$         | 5.0      | 4.1     | 0.5       | 24.0    |
| Number of bunches                    | 42       | 14      | 1920      | 40      |
| Total current /mA                    | 44       | 12      | 200       | 200     |
| Bunch separation /m                  | 28.78    | 3       | 1.2       | 57.6    |
| /ns                                  | 96       | 10      | 4         | 192     |
| Emittance $\epsilon_x$ /nm           | 23       | 23      | 1         | 1       |
| $\epsilon_y$ /nm                     | 0.3      | 0.3     | 0.01      | 0.01    |
| Tune $Q_x$                           | 25       | 25      | 36        | 36      |
| $Q_y$                                | 23       | 23      | 31        | 31      |
| $Q_s$                                | 0.06     | 0.06    | 0.05      | 0.05    |
| Momentum compaction / $10^{-3}$      | 2.52     | 2.52    | 1.2       | 1.2     |
| Beta-functions $\beta_x$ /m          | 18       | 18      | 15        | 15      |
| $\beta_y$ /m                         | 19       | 19      | 15        | 15      |
| Beam size $\sigma_x$ / $\mu\text{m}$ | 643      | 643     | 122       | 122     |
| $\sigma_y$ / $\mu\text{m}$           | 75       | 75      | 12        | 12      |
| Bunch length /mm                     | 7        | 7       | 12        | 12      |

Table 1: Assumed PETRA II and PETRA III parameters. These parameter sets are used in this report for the simulation of the electron cloud build-up.

operation parameters when PETRA is running as a preaccelerator for HERA. The injection energy of PETRA is 7 GeV. The beam is ramped up to an energy

of 12 GeV and transferred into HERA. This operation mode requires a multi-bunch feedback to damp the transverse bunch oscillations. The presently installed feedback system requires a bunch spacing of at least 96 ns due to bandwidth limitations. During machine studies it has been demonstrated that it is possible to operate PETRA with a bunch spacing of only 10 ns but with only 14 bunches without any feedback. The beam marker and bunch signals are shown in Fig. 4 (measured on Feb. 2, 2003). This fill-pattern of PETRA has also been used for some electron cloud simulations to investigate the dependence of the electron cloud density on the bunch to bunch spacing. For PETRA III two parameter sets

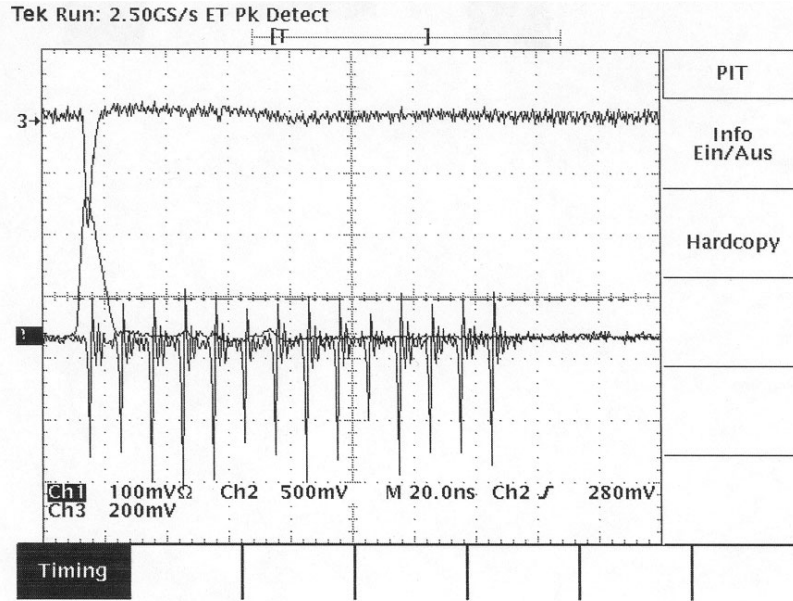


Figure 4: Beam marker and bunch signals at PETRA II. Fourteen bunches with a spacing of only 10 ns are filled in the PETRA ring.

are considered (labeled A and B ) with the same total current but with different number of bunches and bunch spacings. It is planned to operate PETRA III predominantly in mode A. The short bunch spacing in mode A of only 4 ns is a concern with respect to the build-up of electron clouds.

### 2.1.2 PETRA III beam optics

The horizontal and vertical beta-function of a standard PETRA III arc cell and a DBA (double bend achromat) cell of the new ring section [13] are shown in Fig. 5 and Fig. 6. The standard arc cell is a simple FODO cell with a phase advance of  $72^\circ$ . The bending radius  $\rho_B$  of the 5.378 m long dipole magnet is  $\rho_B = 191.729$  m. This arc cell is identical to the presently used cell of the PETRA II ring for synchrotron radiation operation. The dipole magnet of the

planned DBA-cell is only 1 m long (bending radius  $\rho = 22.918$  m) to provide sufficient space for the installation of an undulator magnet.

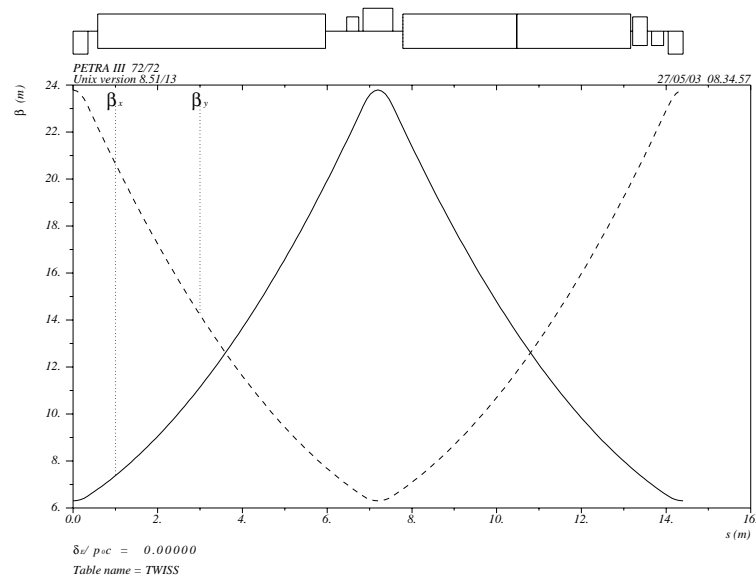


Figure 5: Optics of the standard PETRA III arc cell. The horizontal and vertical beta-functions are plotted versus the position.

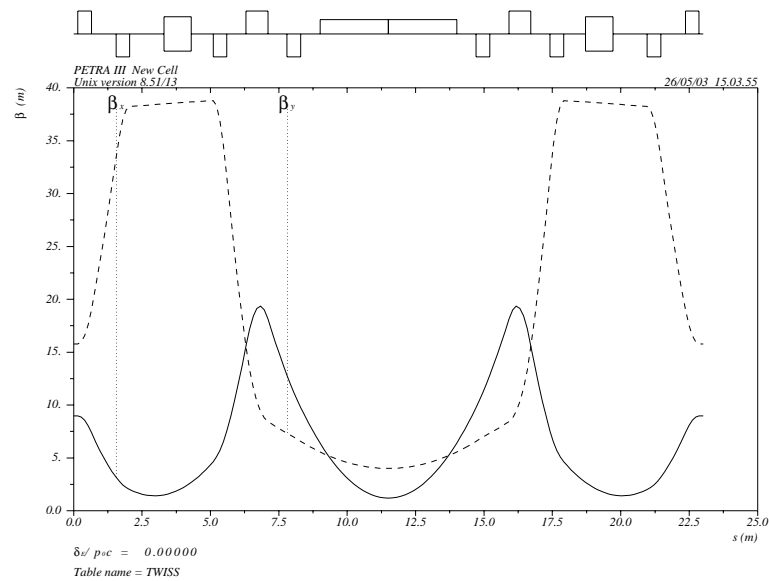


Figure 6: Optics of one cell of the new section of the PETRA III ring.

## 2.2 The vacuum chamber

The geometry of the vacuum chamber in the PETRA II arc is shown in Fig. 7. The chamber has a octagonal shape which may be approximated with ellipses as shown in Fig. 8. The semi axes of the inner (dotted line) ellipse have the same dimensions of half of the actual chamber width and height, while the vertical semi axis of the outer (solid line) ellipse is 35 mm, which is 7 mm larger than the actual chamber half height. For the computer simulations with the ECLOUD2.3 code a chamber boundary is used which is a combination of a straight line and a short arc of the outer ellipse. The boundary is shown in Fig. 9. The vacuum chamber of the synchrotron light source PETRA III is still in the design phase. One possible layout of the chamber in the arc is shown in Fig. 10. The beam chamber has an elliptical shape with semi axes of 20 mm vertically and 40 mm horizontally. An ante-chamber is housing the integrated vacuum pumps. For the simulations of the electron cloud effects only the central chamber is considered. All chamber dimensions are summarized in Tab. 2. Additionally several charge

|  | PETRA II |       | PETRA III |       |
|--|----------|-------|-----------|-------|
|  | 96 ns    | 10 ns | A         | B     |
| horizontal semi axis /mm   | 57       |       | 40        |       |
| vertical semi axis /mm   | 28       |       | 20        |       |
| chamber area /cm <sup>2</sup>                                    | 55.8     |       | 25.1      |       |
| Bunch Population $N_0 / 10^{10}$                                 | 5.0      | 4.1   | 0.5       | 24.0  |
| Bunch separation $d/m$   | 28.78    | 3     | 1.2       | 57.6  |
| /ns  | 96       | 10    | 4         | 192   |
| average bunch charge densities:                                  |          |       |           |       |
| volume $\langle \rho_b \rangle / (10^{12} \text{ m}^{-3})$       | 0.31     | 2.47  | 1.66      | 1.66  |
| line $N_0/d / (10^{10} \text{ m}^{-1})$                          | 0.17     | 1.37  | 0.42      | 0.42  |
| Beam size $\sigma_x / \mu\text{m}$                               | 643      | 643   | 122       | 122   |
| $\sigma_y / \mu\text{m}$   | 75       | 75    | 12        | 12    |
| Bunch length $\sigma_z / \text{mm}$                              | 7        | 7     | 12        | 12    |
| Bunch line charge density $\lambda_b / (10^{12} \text{ m}^{-1})$ | 2.85     | 2.33  | 0.166     | 7.98  |
| Neutrality   |          |       |           |       |
| line charge density $\lambda_n / (10^5 \text{ m}^{-1})$          | 0.96     | 7.53  | 0.156     | 0.156 |

Table 2: Vacuum chamber dimensions and beam charge densities of PETRA II and PETRA III.

densities are listed in Tab. 2 which give first estimates for the expected electron cloud density if one assumes that regardless of the details of the cloud build-up the electron cloud will finally neutralise the average (positron) beam charge density. First the average beam charge volume density is calculated:

$$\langle \rho_b \rangle = \frac{N_0}{Ad},$$





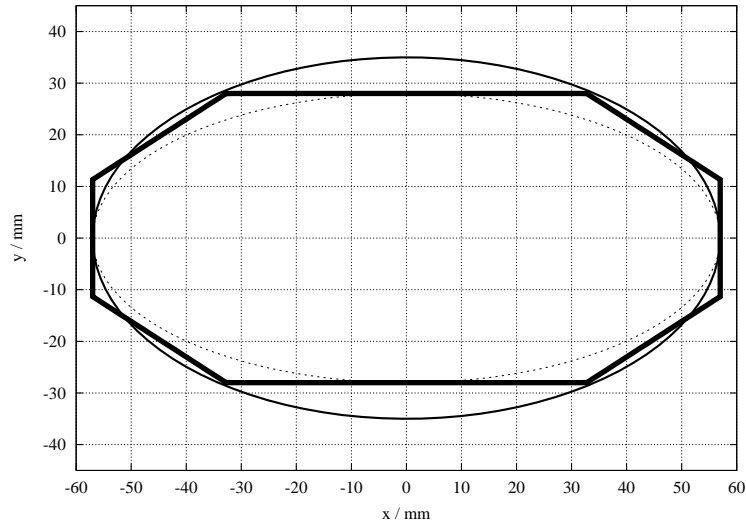


Figure 8: Approximation of the PETRA II chamber with ellipses.

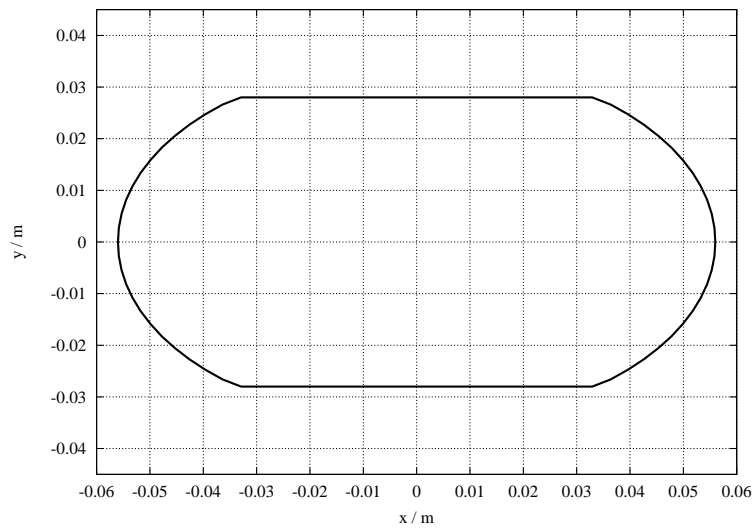


Figure 9: Boundary of the PETRA II chamber used for simulations with the ECLOUD code.

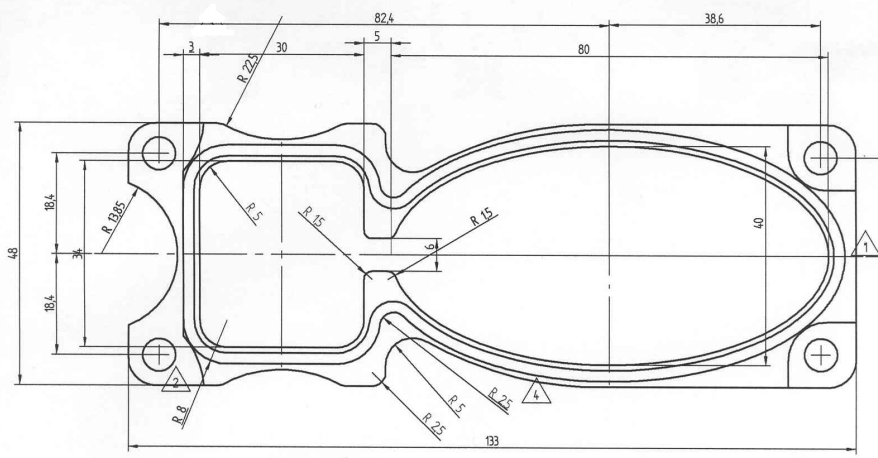


Figure 10: One possible design of the vacuum chamber of the planned PETRA III ring.

## 2.3 Photoelectrons and secondary emission

### 2.3.1 Photoelectrons

A relativistic electron or positron which is bent by a magnetic field will radiate electromagnetic fields or in a quantum view will emit photons. The mean number of photons emitted per length is given as:

$$\frac{dN_\gamma}{dz} = \frac{5}{2\sqrt{3}} \alpha_f \frac{E}{m_0 c^2} \frac{1}{\rho}, \quad (1)$$

where  $E$  is the energy of the positron beam,  $m_0$  the rest mass of the electron,  $\rho$  the bending radius of the dipole magnet and  $\alpha_f = e^2/(4\pi\epsilon_0\hbar c) \approx 1/137$ . Photoelectrons are emitted from the chamber walls at a rate of

$$\frac{dN_{e^-}}{dz} = Y_{eff} \frac{dN_\gamma}{dz}, \quad (2)$$

where  $Y_{eff}$  is the effective photoelectron emission yield. The total number of photoelectrons per length generated from one bunch is  $N_0 dN_{e^-}/dz$ , where  $N_0$  is the bunch population. The effective photoelectron emission yield depends on the photon spectrum, the photoelectric yield of the material and on the photon reflectivity of the chamber.

The photoelectric yield of Aluminum as a function of the photon energy  $\eta_{pe}(u)$  shown in Fig. 11 for normal incidence is obtained from reference [14], which is based on the results of measurements.

The power spectrum of the photons is given by [15, 16]:

$$\mathcal{P}(\omega) = \frac{P_\gamma}{\omega_c} S(\omega/\omega_c) \quad (3)$$

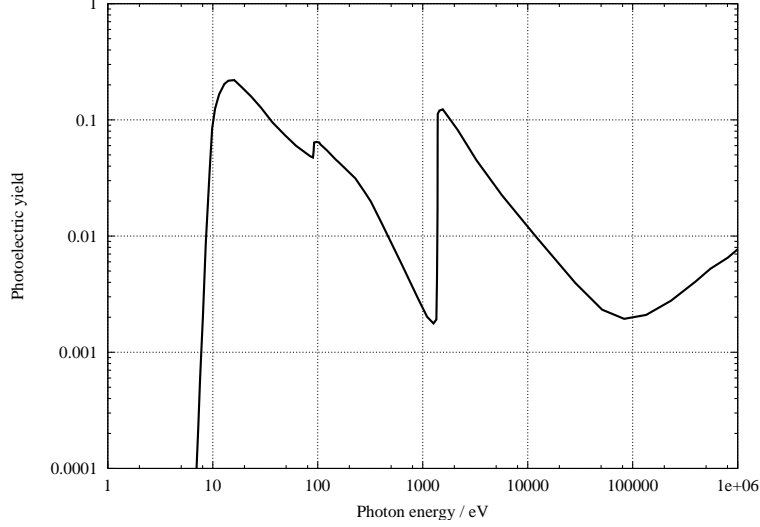


Figure 11: Photoelectric yield of Aluminum for normal incidence.

where the function  $S(x)$  is defined as

$$S(x) = \frac{9\sqrt{3}}{8\pi} x \int_x^\infty d\zeta K_{\frac{5}{3}}(\zeta), \quad (4)$$

using the Bessel function of the third kind of order  $5/3$ . Furthermore,  $\omega_c = (3/2)(c/\rho)\gamma^3$  is the critical frequency of the photons, and  $P_\gamma = \int_0^\infty d\omega \mathcal{P}(\omega)$  the total power.

The photon density  $n(u)$  as a function of the photon energy  $u$  is obtained from the power spectrum:

$$n(u) = \frac{1}{u} \frac{1}{\hbar} \mathcal{P}(u/\hbar), \quad (5)$$

which can be rewritten as

$$n(u) = \frac{P_\gamma}{u_c^2} F(u/u_c), \quad (6)$$

where  $F(x) = S(x)/x$  and  $u_c = \hbar\omega_c$  is the critical energy of the photons. The power spectrum  $S(u/u_c)$  and the photon density  $F(u/u_c)$  are show in Fig. 12. (One obtains for the integrals:  $\int_0^\infty ds S(x) = 1$  and  $\int_0^\infty ds F(x) = 15\sqrt{3}/8$ .)

The effective photoelectron emission yield for normal incidence  $Y_\perp$  can be calculated as:

$$\begin{aligned} Y_\perp &= \frac{\int_0^\infty du \eta_{pe}(u) n(u)}{\int_0^\infty du n(u)}, \\ &= \frac{8}{15\sqrt{3}} \int_0^\infty \frac{du}{u_c} \eta_{pe}(u) F(u/u_c). \end{aligned} \quad (7)$$

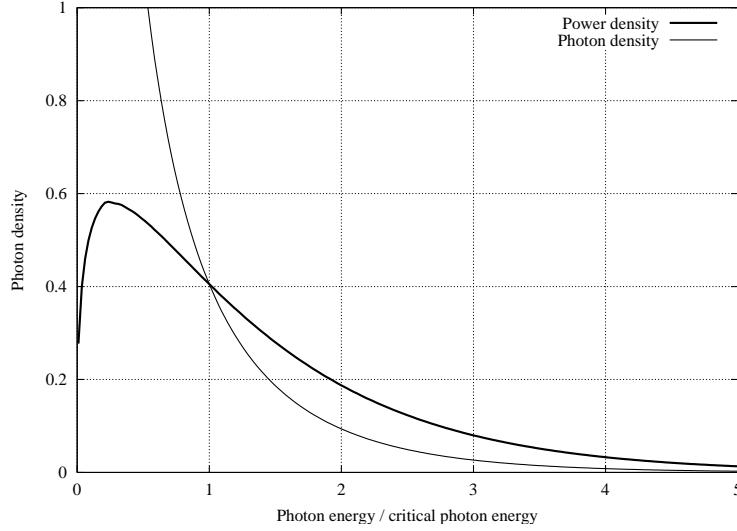


Figure 12: Number of photons per energy and photon power spectrum.

A plot of photoelectron yield times the photon density  $F(u/u_c)$  is shown in Fig. 13 for a critical energy of about 2.5 keV corresponding to a beam energy of 6 GeV and a bending radius of about 192 m. For these parameters one obtains an effective photoelectron emission yield of about 0.05 for normal incidence photons (see Tab. 3).

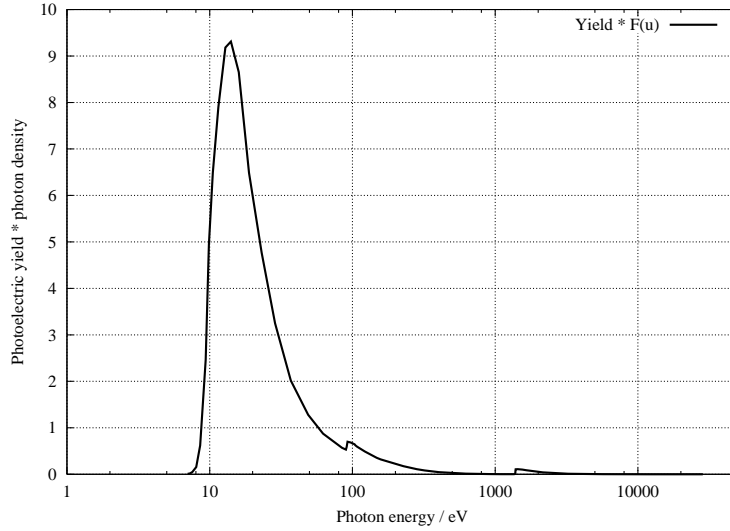


Figure 13: The product of the photoelectric yield of Aluminum and the photon density for a beam energy of 6 GeV.

The effective photoelectron yield for photons at grazing incidence can either be significantly enhanced or reduced, depending on the reflection coefficient of

|                         | PETRA II | PETRA III |
|-------------------------|----------|-----------|
| Energy /GeV             | 7        | 6         |
| Bending radius $\rho/m$ | 191.729  | 191.729   |
| $u_c$ /keV              | 3.968    | 2.499     |
| $Y_{\perp}$             | 0.047    | 0.042     |

Table 3: Effective photoelectron yield for normal incidence.

the photons [14, 17, 18] which is difficult to know precisely. The number of photoelectrons in the vacuum chamber will be reduced for chamber designs with an ante-chamber. As a result of these unknown factors the precise value for the effective photoelectron yield is not know. For most of the simulations an effective photoelectron yield of

$$Y_{eff} \approx 0.1 \quad (8)$$

will be used, which is about a factor of two larger than that calculated for normal incidence photons assuming that no ante-chamber is present. An effective photoelectron yield of 0.1 is reported also for the KEK B-factory [19] vacuum chamber. For some of the simulations an even higher photoelectron yield of  $Y_{eff} = 1$  is used to examine the dependence of the electron cloud density on the number of primary generated photoelectrons. The photoelectron emission rates are summarized for PETRA II and PETRA III in Tab. 4.

|                                  | PETRA II |         | PETRA III |         |
|----------------------------------|----------|---------|-----------|---------|
|                                  | 96 ns    | 10 ns   | A         | B       |
| Energy /GeV                      | 7        | 7       | 6         | 6       |
| Bunch Population $N_0/10^{10}$   | 5.0      | 4.1     | 0.5       | 24.0    |
| Bending radius $\rho/m$          | 191.729  | 191.729 | 191.729   | 191.729 |
| $dN_{\gamma}/dz$ / m             | 0.753    | 0.753   | 0.645     | 0.645   |
| $Y_{eff}$                        | 0.1      | 0.1     | 0.1       | 0.1     |
| $dN_{e-}/dz$ / m                 | 0.075    | 0.075   | 0.065     | 0.065   |
| $N_0 dN_{e-}/dz$ /( $10^{10}$ m) | 0.376    | 0.309   | 0.032     | 1.549   |

Table 4: Photoelectron emission rates for PETRA II and PETRA III.

### 2.3.2 Secondary emission

The mean energy of the (primary) photoelectrons is about 7 eV. The electric field of the trailing bunches will accelerate the photoelectrons up to several hundred eV depending on the bunch population and the chamber dimensions. A photoelectron which hits the vacuum chamber wall can generate secondary electrons with a secondary emission yield  $\delta_{SE}(E)$  which depends on the energy of the primary electron and on the material properties. The following data enter into the simulation recipe of the ECLLOUD 2.3 code [12].

The measured data [20] for the secondary emission yield can be described analytically, as suggested by M. Furman [21], in the following way:

$$\delta_{SE}(E) = \delta_{max} \frac{s (E/E_{max})}{s - 1 + (E/E_{max})^s}, \quad (9)$$

with three material dependent parameters  $\delta_{max}$ ,  $E_{max}$  and  $s$ , which depend on the angle of incidence of the primary electron with respect to the material surface. The secondary emission yield of a non pure (technical) material depends strongly on the surface properties of the material. Various surface treatments have been investigated [22] to reduce the secondary emission yield. A very powerful method to circumvent the problems due to electron multiplication is the "dose effect" (or processing). Typical parameters for copper and aluminum after processing are given in Tab. 5. Copper "as received" may have a secondary emission parameter  $\delta_{max}$  of more than 2.0 and aluminum "as received" of more than 3.0. With a

|                       | Cu   | Al   |
|-----------------------|------|------|
| $\delta_{max}$        | 1.4  | 2.2  |
| $E_{max} / \text{eV}$ | 240  | 300  |
| $s$                   | 1.39 | 1.35 |

Table 5: Parameters for the secondary emission yield for copper and aluminum (normal incidence).

certain probability the primary electrons which hit the surface interact in an inelastic way with the material yielding "true secondary" electrons. But some electrons are elastically backscattered off the surface. The Eqn. (9) refers to the true secondary electron yield which is plotted in Fig. 14 as solid curves for copper and aluminum using the parameters from Tab. 5. The total secondary emission yield can be written as a sum of the true secondary electron yield and the reflected electron yield:

$$\delta_{tot}(E) = \delta_{SE}(E) + \delta_R(E) = \delta_{SE}(E) \frac{1}{1 - f_R(E)}, \quad (10)$$

where the factor  $f_R(E)$  gives the yield from reflected electrons as a fraction of the total yield ( $\delta_{tot} = f_R \delta_{SE}$ ). The fraction of reflected electrons has been measured as a function of the primary energy. A fit to the data gives for primary energies below 300 eV [20]:

$$f_R(E) = \exp \left( A_0 + A_1 \ln(B + E/\text{eV}) + A_2 (\ln(B + E/\text{eV}))^2 \right), \quad (11)$$

with  $A_0 = 20.7$ ,  $A_1 = -7.08$ ,  $A_2 = 0.484$  and  $B = 56.9$ . The total secondary emission yield is plotted in Fig. 14 as dashed curves for copper and aluminum. The reflected component contributes significantly to the total secondary electron

yield for primary electron energies of a few eV. Besides the true secondary and reflected electrons there is a third component to the total secondary electron yield, which is referred to as "rediffused" electrons. These are electrons which penetrate into the material and undergo multiple scattering inside the material before being reflected back out the material. This component is neglected in simulations with EPCLOUD 2.3. The energy distribution of the true secondary

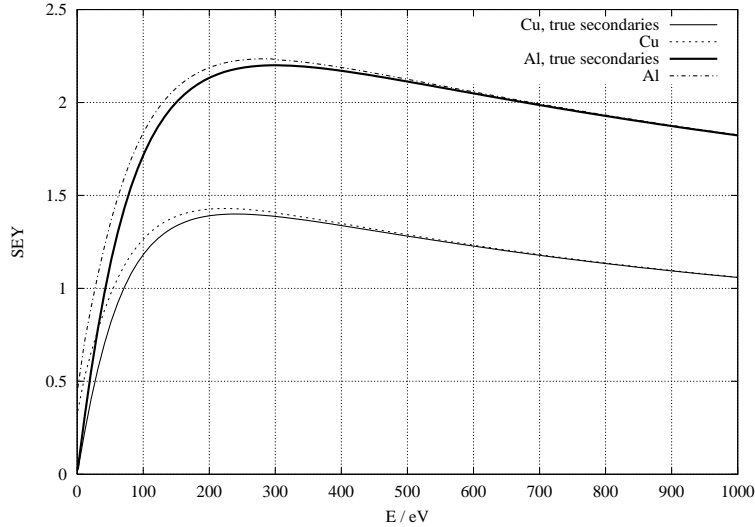


Figure 14: Secondary emission yield for copper and aluminum vacuum chambers. The contribution from the reflected electrons is included in the total yield presented with the dashed curves.

electrons is fitted with the following formula [23]:

$$D(E) = C \exp\left(-\frac{(\ln(E/E_0))^2}{2\tau^2}\right), \quad (12)$$

where  $C$ ,  $\tau$  and  $E_0$  are parameters to fit the measured data. The energy distribution is plotted in Fig. 15 for  $C = 0.2$ ,  $\tau = 1$  and  $E_0 = 1.8$  eV. The slight dependence of the parameters on the energy of the primary electron is neglected here. The average energy of a true secondary electron is about 3.5 eV.



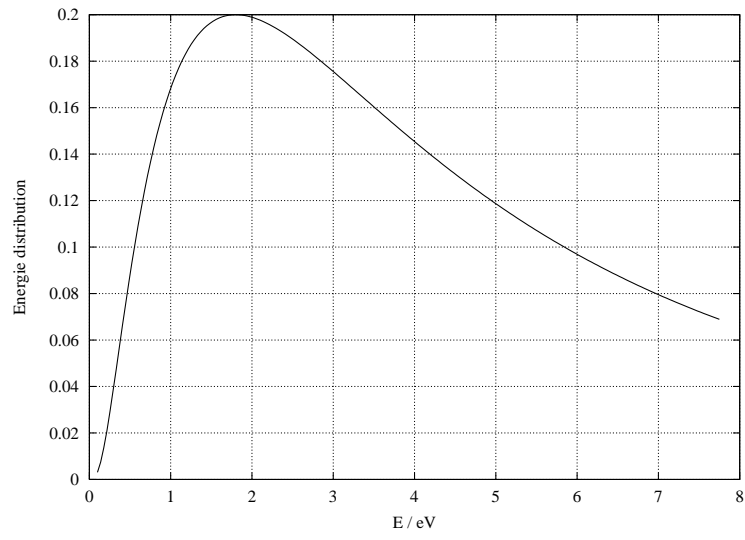


Figure 15: Energy distribution of secondary electrons.

### 3 Simulation of the electron cloud build-up

For all electron cloud simulations the code E CLOUD 2.3 has been used [12]. The beam parameters and the vacuum chamber dimensions have been taken from Tab. 1 and Tab. 2. If not stated otherwise the photoelectron emission rates are based on an effective photoelectron yield of 0.1 (see Tab. 4). The parameters for the secondary emission yield for a aluminum chamber with maximum yield  $\delta_{max}$  of 2.2 have been assumed (see Tab. 5) for PETRA II and PETRA III. Plots of the electron cloud population and the electron cloud density in the bunch center are presented in the following subsections. The results are summarized in a table at the end of this section.

#### 3.1 PETRA II

##### 3.1.1 PETRA II – Standard fill with 96 ns bunch spacing

In the PETRA II storage no performance degradations due to electron clouds have been observed during the standard operation mode with a bunch spacing of 96 ns. The simulation (using the E CLOUD 2.3 code) predicts an electron cloud build-up during about  $5 \times 95$  ns to a total cloud population of  $0.46 \cdot 10^{10}$  electrons per meter as shown in Fig. 16. This corresponds to an average cloud density of  $0.83 \cdot 10^{12} \text{ m}^{-3}$ . The electron cloud center density, as obtained from

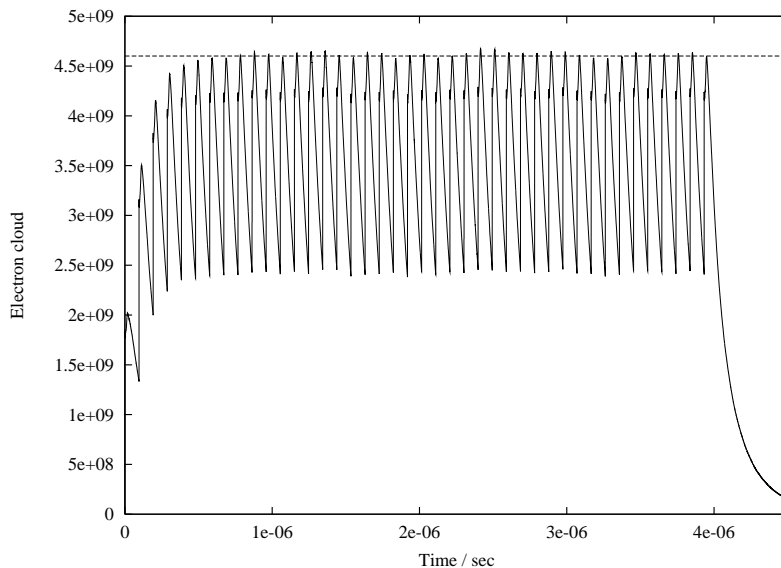


Figure 16: Simulated population of the electron cloud build-up in the PETRA II vacuum chamber using E CLOUD 2.3. The dashed line indicates a population of  $0.46 \cdot 10^{10}/\text{m}$ .

simulations, is plotted in Fig. 17 and for a time interval of one microsecond in

Fig. 18. Although there are fluctuations the electron center density is found to be about  $0.7 \cdot 10^{12} \text{ m}^{-3}$  as indicated in Fig. 18.

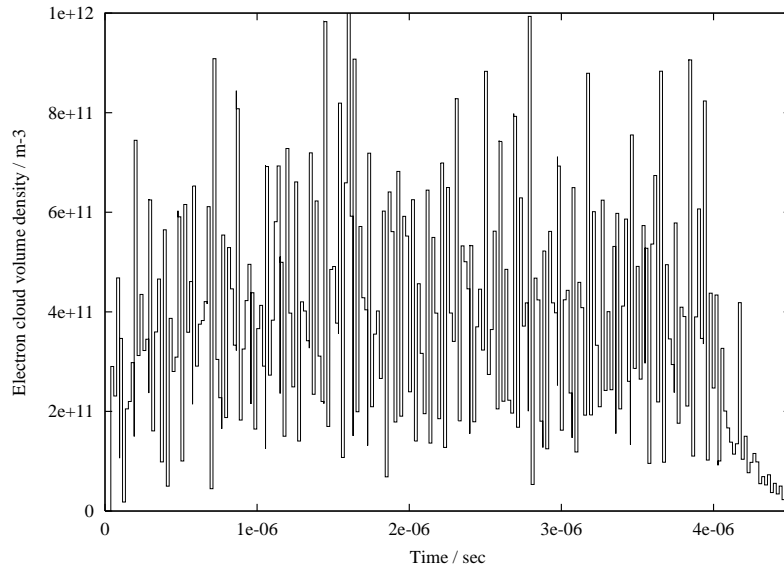


Figure 17: Electron cloud center density in the PETRA II vacuum chamber (results from ELOUD 2.3).

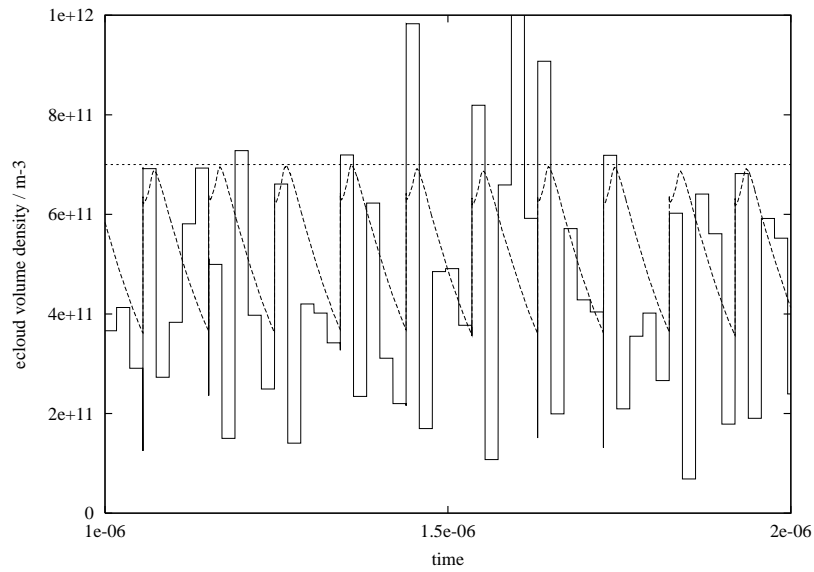


Figure 18: Detail of electron cloud center density in the PETRA II vacuum chamber (results from ELOUD 2.3). The cloud population is also shown for reference, plotted in arbitrary units (dashed line). The dashed line indicates a density of  $0.7 \cdot 10^{12} \text{ m}^{-3}$ .

### 3.1.2 PETRA II – Special fill with 10 ns bunch spacing

During machine studies PETRA II was operated with a special fill pattern with a bunch spacing of only 10 ns. The simulation of the electron cloud population in this case is shown in Fig. 19. At the end of the bunch train a population of  $1.4 \cdot 10^{10}$  electrons per meter is reached, corresponding to an average electron cloud density of  $2.5 \cdot 10^{12} \text{ m}^{-3}$ , which is about a factor of 3.5 higher than in the standard fill pattern with 96 ns bunch spacing. The equilibrium electron cloud population is not reached within the short bunch train of only 14 bunches. A short gap is sufficient to let the cloud population decay by a factor of two. The

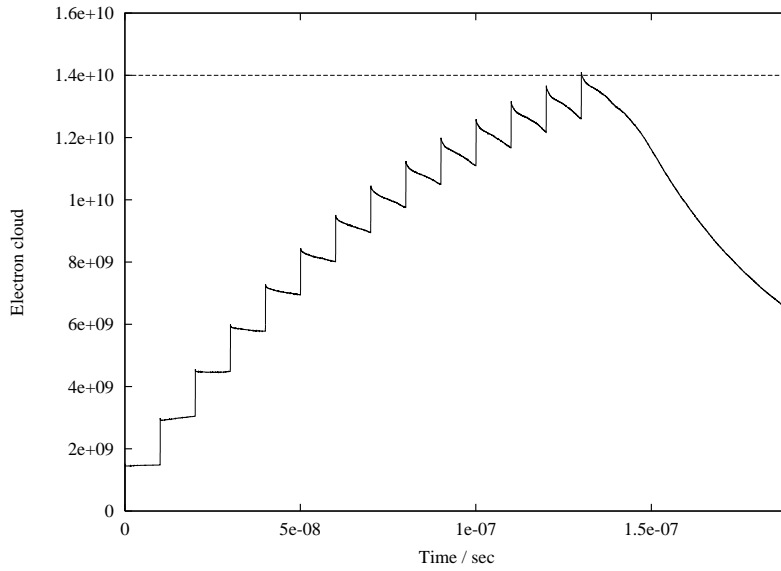


Figure 19: Simulated population of an electron cloud in the PETRA II (10 ns) vacuum chamber using ECLLOUD 2.3.

simulation result for the electron cloud center density is shown in Fig. 20. As indicated by the dashed line in the figure a center density of about  $2.1 \cdot 10^{12} \text{ m}^{-3}$  is reached at the end of the bunch train. The center density and the average density do not differ significantly and are similar to the neutrality density of  $2.4 \cdot 10^{12} \text{ m}^{-3}$  (see Tab. 2).

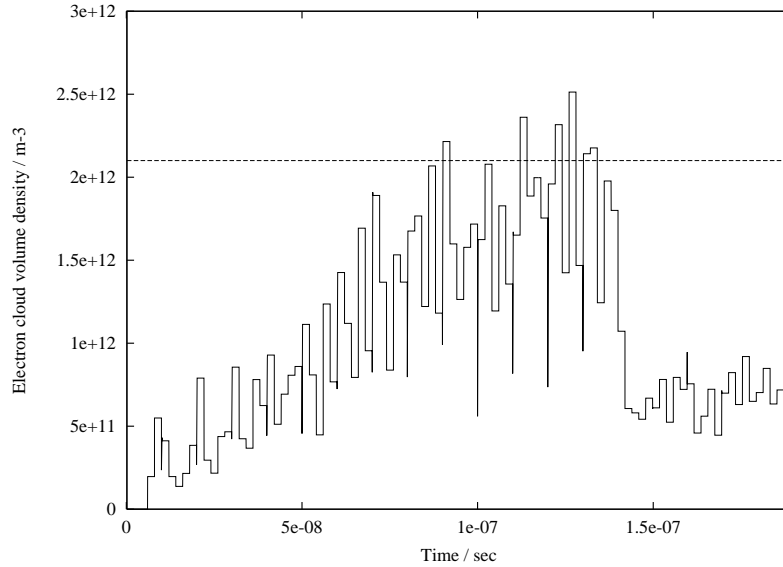


Figure 20: Electron cloud center density in the PETRA II (10 ns) vacuum chamber using ELOUD 2.3. The dashed line indicates a density of  $2.1 \cdot 10^{12} \text{m}^{-3}$ .

### 3.2 PETRA III

The two parameter sets for PETRA III (labeled A and B, see Tab. 1) have been considered for the simulations with the ELOUD 2.3 code. Fig. 21 shows the distribution of the macro particles in the elliptical vacuum chamber at different time steps during the simulation. The electron cloud population, average and center cloud densities are presented in the following subsections.

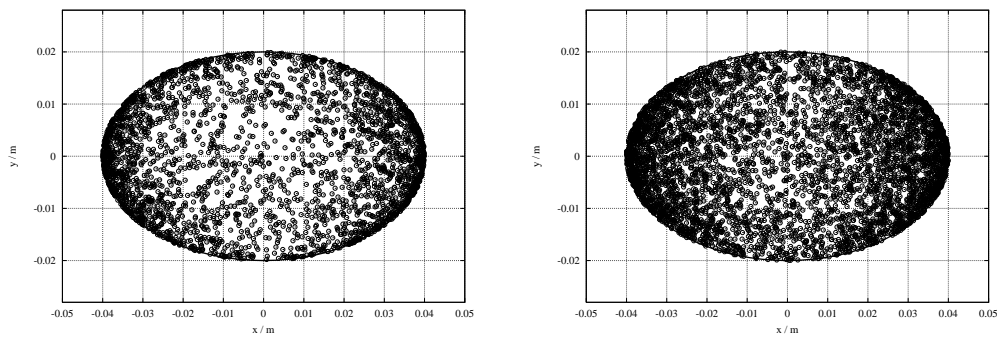


Figure 21: Simulation of an electron cloud build-up in the PETRA III vacuum chamber using ELOUD 2.3. The macro particle distributions at two different times are shown in the two graphs.

### 3.2.1 PETRA III – Variant A

First the parameter set A with many bunches and a small bunch spacing of only 4 ns is considered. The build-up of the electron cloud population simulated with the ECLLOUD 2.3 code is shown in Fig. 22. A equilibrium population of about  $3.2 \cdot 10^{10}$  is reached after about 100 bunches of the bunch train. This corresponds to an average electron cloud population of  $1.3 \cdot 10^{12} \text{ m}^{-3}$ . The corresponding

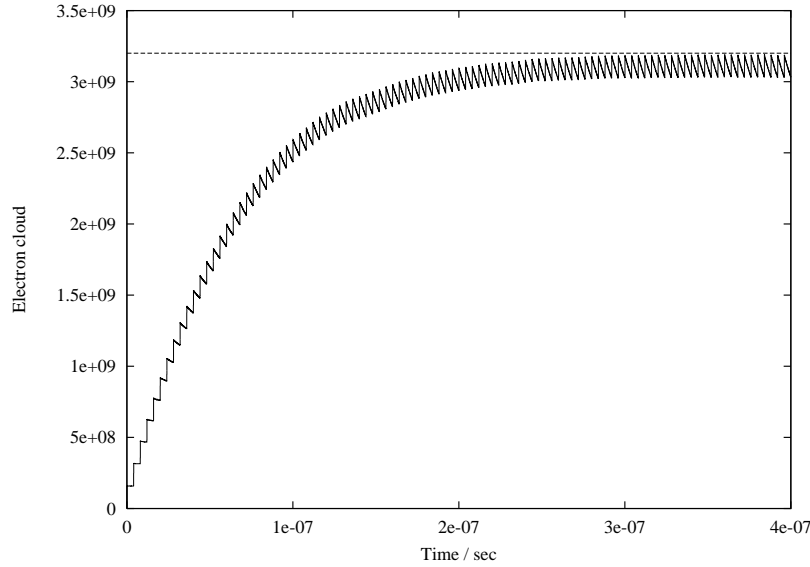


Figure 22: Simulation of the electron cloud population in the PETRA III-A vacuum chamber using ECLLOUD 2.3. The dashed line indicates an electron cloud population of  $0.32 \cdot 10^{10}$ .

results for the electron cloud center density are show in Fig. 23 and in detail for a shorter time interval in Fig. 24. The center density of about  $1.0 \cdot 10^{12} \text{ m}^{-3}$  is almost equal to the average electron cloud density.

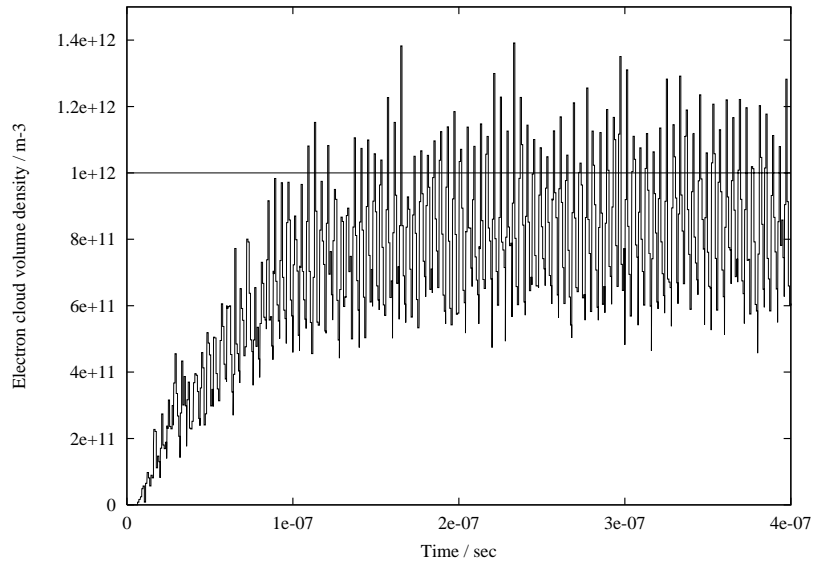


Figure 23: Simulation of the electron cloud center density in the PETRA III-A vacuum chamber using ECLLOUD 2.3.

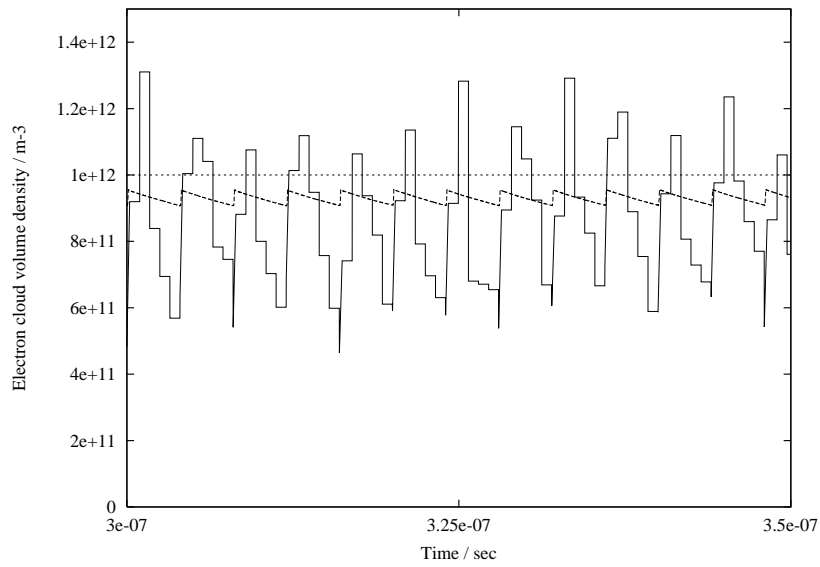


Figure 24: Detail of the electron cloud center density in the PETRA III-A vacuum chamber using ECLLOUD 2.3.

### Simulations with a effective photoelectron yield of 1.0.

An effective photoelectron yield of 0.1 has been normally assumed for the simulations. To study the dependence of the electron cloud density on this parameter the previous simulations of PETRA III (variant A) has been repeated with a photoelectron yield of 1.0 and with otherwise unchanged parameters. The results for the bunch population are shown in Fig. 25. The electron cloud population is  $1.5 \cdot 10^{10}$  per meter for this case, which is a factor of 4.7 higher compared with the previous simulation with a ten times lower photoelectron yield. The correspond-

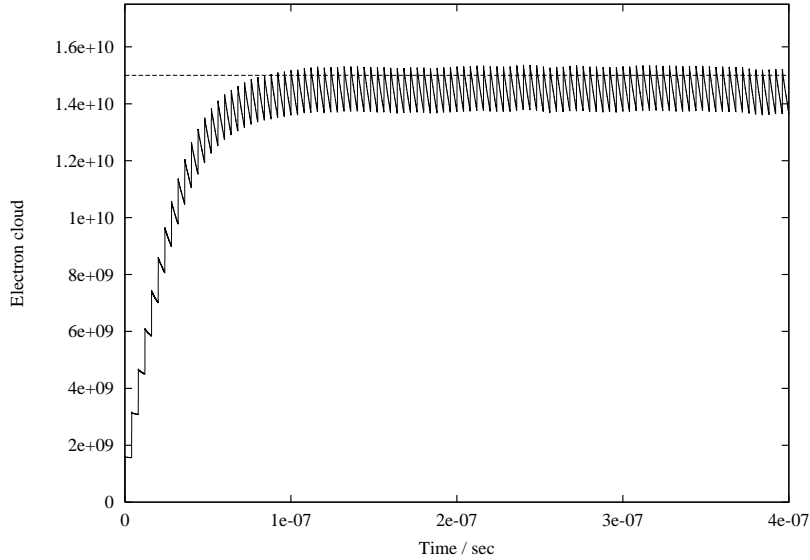


Figure 25: Simulation of the electron cloud population in the PETRA III-A vacuum chamber using ECLOUD 2.3. The line indicates an electron cloud population of  $1.5 \cdot 10^{10}$ . A photoelectron yield of 1.0 has been assumed.

ing center density of the electron cloud is shown in Fig. 26. The line indicates a center density of  $3.5 \cdot 10^{12} \text{ m}^{-3}$  which is a factor 3.5 higher than in the case with a photoelectron yield of 0.1.



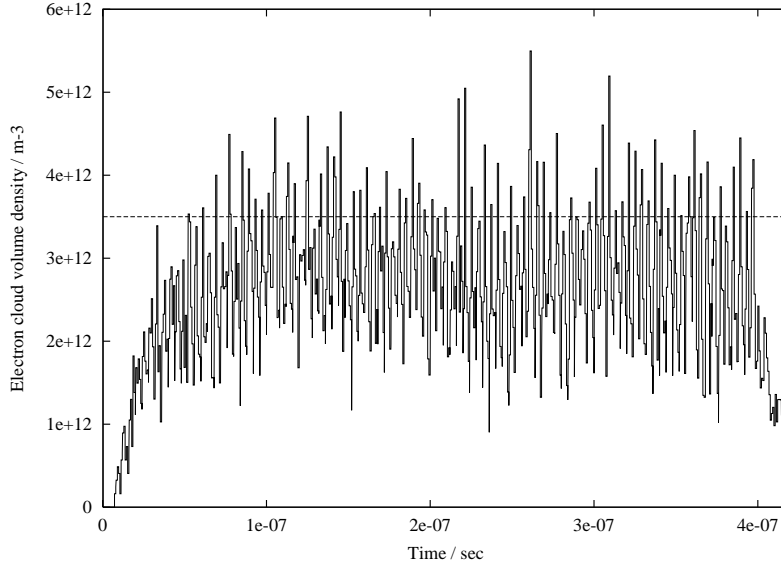


Figure 26: Simulation of the electron cloud center density in the PETRA III-A vacuum chamber using ECLLOUD 2.3. A photoelectron yield of 1.0 has been assumed.

### 3.2.2 PETRA III – Variant B

No electron cloud build-up over the bunch train is found in the simulation results for a large bunch spacing of 192 ns (parameter set B). Each bunch induces an electron cloud with a population of about  $2.2 \cdot 10^{10}$  which decays before the next bunch of the train arrives. This corresponds to an average electron density of  $8.7 \cdot 10^{12} \text{ m}^{-3}$ . A center density of about  $1.5 \cdot 10^{12} \text{ m}^{-3}$  is found from the simulations (see Fig. 28).

### 3.2.3 Summary of the PETRA simulation results

The previously discussed results are summarized in Tab. 6 for the reference parameter set with an photoelectron yield of 0.1. The average electron cloud density has been calculated from the electron cloud population and the vacuum chamber dimensions.

One simulation for PETRA III (variant A) has been done with an photoelectron yield of 1.0. For that case a cloud population of  $1.5 \cdot 10^{10}$ , corresponding to an average cloud density of  $5.96 \cdot 10^{12} \text{ m}^{-3}$ , was obtained. The center density was  $3.5 \cdot 10^{12} \text{ m}^{-3}$ .

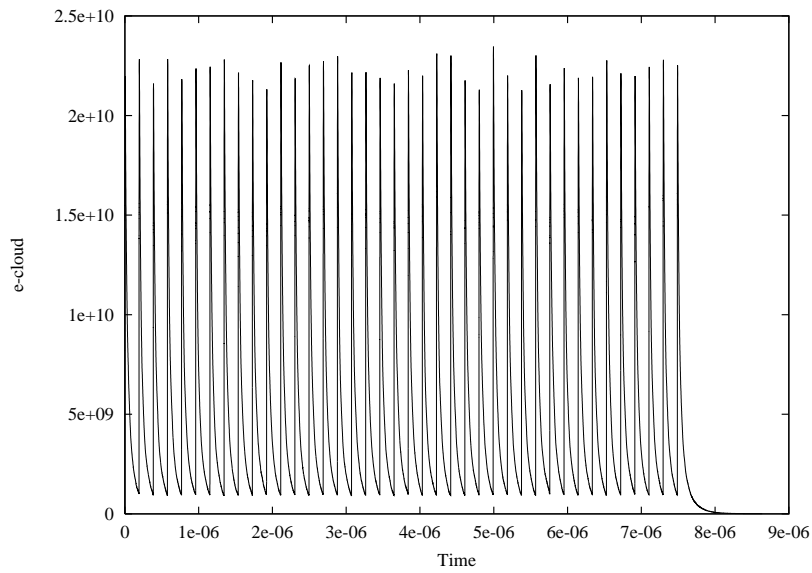


Figure 27: Simulation of the electron cloud population in the PETRA III-B vacuum chamber using ECLLOUD 2.3.

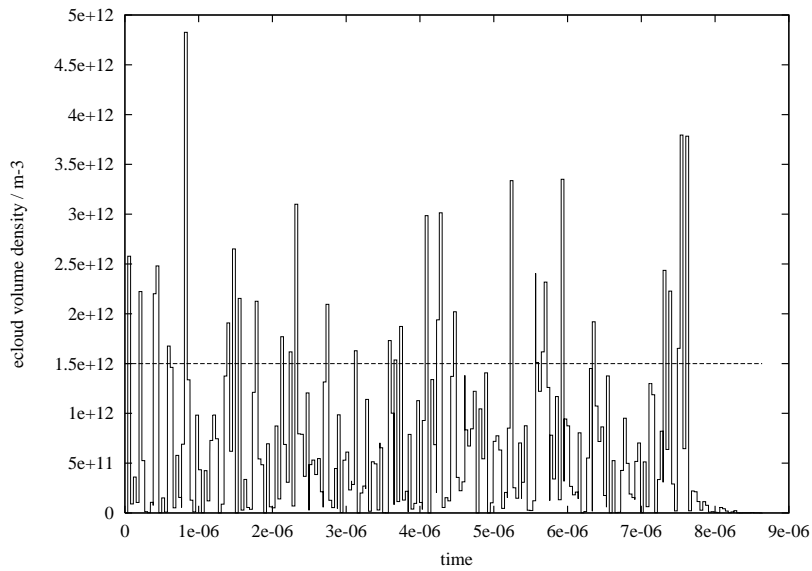


Figure 28: Simulation of the electron cloud center density in the PETRA III-B vacuum chamber using ECLLOUD 2.3.

|   | PETRA II |       | PETRA III |      |
|---|----------|-------|-----------|------|
|   | 96 ns    | 10 ns | A         | B    |
| chamber area /cm <sup>2</sup>   | 55.8     |       | 25.1      |      |
| Bunch Population $N_0 / 10^{10}$  | 5.0      | 4.1   | 0.5       | 24.0 |
| Bunch separation /ns  | 96       | 10    | 4         | 192  |
| average bunch charge densities:<br>volume $\langle \rho_b \rangle / (10^{12} \text{ m}^{-3})$ | 0.31     | 2.47  | 1.66      | 1.66 |
| Results from the simulations  |          |       |           |      |
| Cloud Population / $10^{10}$ / m  | 0.46     | 1.4   | 0.32      | 2.2  |
| Average density /( $10^{12} \text{ m}^{-3}$ )   | 0.83     | 2.5   | 1.3       | 8.7  |
| Center density / ( $10^{12} \text{ m}^{-3}$ )   | 0.7      | 2.1   | 1.0       | 1.5  |

Table 6: Beam and cloud charge densities for PETRA II and PETRA III.

### 3.3 KEK-B LER

A vertical emittance growth due to an instability caused by electron clouds has been observed in the low energy ring (LER) of the KEK B-Factory for beam intensities above 500 mA in the case that no solenoids are switched on as a countermeasure [2, Fig. 16]. The code E-CLOUD 2.3 has also been used to simulate the build-up of the electron cloud in the KEKB LER using the parameters from Tab.7 and 8, which have been compiled from [24, 2].

|   | KEK-B LER |
|---|-----------|
| Energy /GeV                                     | 3.5       |
| Circumference /m                                | 3016      |
| Bending radius /m                               | 15.9      |
| revolution frequency /kHz                       | 99.4      |
| Bunch Population / $10^{10}$                    | 3.0       |
| Number of bunches                               | 1200      |
| Total current /mA                               | 573       |
| Bunch separation /m                             | 2.39      |
| /ns   | 8         |
| Emittance $\epsilon_x$ /nm                      | 18        |
| $\epsilon_y$ /nm                                | 0.0036    |
| Tune $Q_x / Q_y$                                | 46 / 46   |
| $Q_s$   | 0.01      |
| Momentum compaction / $10^{-4}$                 | $\sim 1$  |
| Beta-functions $\beta_x / \beta_{ey}$ /m /      | 15 / 15   |
| Beam size $\sigma_x / \sigma_y$ / $\mu\text{m}$ | 520 / 7   |
| Bunch length /mm                                | 4         |

Table 7: Assumed KEK B LER parameters (part 1). These parameter sets are used for the simulation of the electron cloud build-up in the KEK B-factory low energy ring.

A secondary emission yield of 1.4 (see Tab.5) has been assumed for the copper chamber. A field free region has been considered for the simulations. The results of the simulation of the electron cloud population are shown in Fig. 29. An equilibrium population of  $2.9 \cdot 10^{10}$  electrons per meter is obtained. This corresponds to an average electron cloud density of  $4.2 \cdot 10^{12} \text{ m}^{-3}$ . The electron cloud center density obtained from the simulation with E-CLOUD 2.3 is shown in Fig. 30. The center density of the cloud is about  $3.0 \cdot 10^{12} \text{ m}^{-3}$ . This is about a factor of three larger than the simulated center density for PETRA III variant A.

| KEK-B LER  |        |
|--|--------|
| Vacuum chamber   |        |
| chamber radius /mm   | 47     |
| chamber area /cm <sup>2</sup>                                    | 69.3   |
| average bunch charge densities:                                  |        |
| volume $\langle \rho_b \rangle / (10^{12} \text{ m}^{-3})$       | 1.8    |
| line $N_0/d / (10^{10} \text{ m}^{-1})$                          | 2.91   |
| Bunch line charge density $\lambda_b / (10^{12} \text{ m}^{-1})$ | 2.99   |
| Neutrality   |        |
| line charge density $\lambda_n / (10^5 \text{ m}^{-1})$          | 0.43   |
| Photoelectron emission rates                                     |        |
| $dN_\gamma/dz / \text{m}$  | 4.538  |
| $Y_{eff}$  | 0.1    |
| $dN_{e^-}/dz / \text{m}$   | 0.4538 |
| $N_0 dN_{e^-}/dz / (10^{10} \text{ m})$                          | 1.362  |

Table 8: Assumed KEK B LER parameters (part 2). These parameters are used for the simulation of the electron cloud build-up in the KEK B-factory low energy ring.

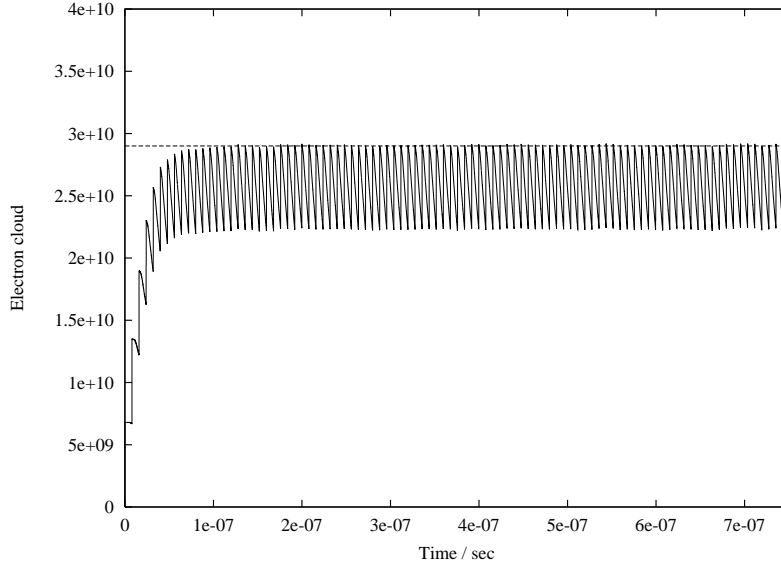


Figure 29: Simulated population of the electron cloud in the KEK-B vacuum chamber using ECLOUD 2.3. The dashed line indicates a population of  $2.9 \cdot 10^{10}$ .

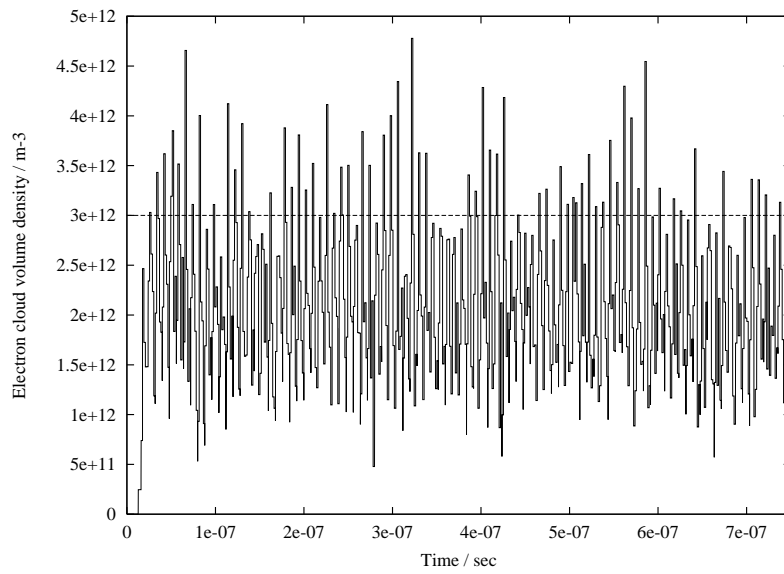


Figure 30: Electron cloud center density in the KEK-B vacuum chamber (results from ELOUD 2.3).

## 4 Single bunch instabilities due to electron clouds

### 4.1 Broad band resonator model

A broad band resonator model has been developed in [25, 26] to characterize the interaction between the positron bunch and the electron cloud. The basic ingredients of the model are the line charge densities  $\lambda_b$  and  $\lambda_c$  of the positron beam and of the electron cloud, and the transverse beam sizes ( $\sigma_x$  and  $\sigma_y$ ). It is assumed that the electron cloud has the same transversal dimensions as the beam. The line charge density of the cloud is therefore  $\lambda_c = 2\pi\sigma_x\sigma_y\rho_c$ , where  $\rho_c$  is the volume charge density in the center of the vacuum chamber obtained from computer simulations. The dipole wake can be written as:

$$w_1(s) = \hat{w}_1 \sin\left(\omega_c \frac{s}{c}\right) \exp\left(-\frac{\omega_c s}{2Qc}\right), \quad (13)$$

with

$$\hat{w}_1 = \frac{\gamma}{r_e c^3} \frac{1}{\lambda_b} \omega_b^2 \omega_c C, \quad (14)$$

and

$$\omega_b^2 = \frac{1}{\gamma} \frac{r_e c^2}{(\sigma_x + \sigma_y) \sigma_y} \lambda_c, \quad \omega_c^2 = \frac{r_e c^2}{(\sigma_x + \sigma_y) \sigma_y} \lambda_b, \quad (15)$$

with  $r_e$  the classical electron radius,  $\gamma$  the beam energy measured in units of the rest mass, and  $C$  the circumference of the ring. The dipole wake within a bunch can be calculated as the convolution integral of the point charge wake  $w_1(s)$  with the Gaussian charge density in the bunch  $g(s) = \exp(-\frac{1}{2}(s/\sigma_z)^2)/(\sigma_z\sqrt{2\pi})$ :

$$W_1(s) = \int_0^\infty d\xi g(s - \xi) w_1(\xi). \quad (16)$$

The "cloud" frequency  $\omega_c$  is the frequency of the broad band resonator. This frequency depends only on the properties of the positron beam. All parameters of the broad band resonator which do not depend directly on the cloud population are summarized in Tab. 9. A Q-value of 5 has been assumed to take into account the broad band characteristic of the impedance.

The normalized point charge wake potential  $w_1(s)/\hat{w}_1$  as well as the bunch wake potential  $W_1(s)/\hat{w}_1$  are shown in Fig. 31 for the PETRA III-A parameters. The dash-dotted line in Fig. 31 shows the charge distribution of the bunch. The effect of the wakefield due to the electron cloud is greatly reduced since the wavelength  $(2\pi c)/\omega_c$  of the point charge wakepotential is smaller than the bunch length. The quantity  $W_1(\sigma_z)/\hat{w}_1$  is the bunch wake potential at the position  $s = \sigma_z$  (tail of the bunch) normalized to the amplitude  $\hat{w}_1$  of the point charge wake potential (see Tab. 9). In a two particle model the quantity  $W_1(\sigma_z)$  is used as an estimate of the wake from the head particle acting on the tail particle.

|   | PETRA II |       | PETRA III |        | KEK-B LER |
|---|----------|-------|-----------|--------|-----------|
|   | 96 ns    | 10 ns | A         | B      | 573 mA    |
| Bunch Population /10 <sup>10</sup>              | 5.0      | 4.1   | 0.5       | 24.0   | 3.0       |
| cloud frequency $\omega_c / (2\pi \text{ GHz})$ | 18.35    | 16.61 | 25.42     | 176.13 | 70.40     |
| $W_1(\sigma_z)/\hat{w}_1$                       | 0.108    | 0.134 | 0.039     | 0.005  | 0.042     |
| Q-value   | $\sim 5$ |       | $\sim 5$  |        | $\sim 5$  |

Table 9: Parameters for the broad band resonator model which depend only on the positron beam properties.

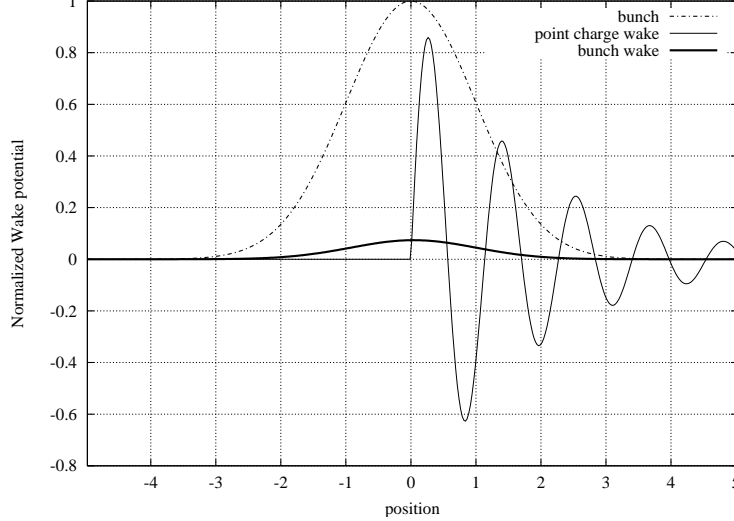


Figure 31: Normalized wake potential of electron clouds in PETRA III (parameter set A). The position within the bunch is measured in units of the rms bunch length  $\sigma_z$ .

## 4.2 Estimates for the instability thresholds

The strong-head tail instability can be treated in a simplified way using a two particle model [27]. The equations of motion during the time  $0 < s/c < T_s/2$ , where  $T_s = 1/f_s$  is the synchrotron oscillation period, are

$$\frac{d^2}{ds^2} y_1 + \left( \frac{\omega_\beta(\delta_1)}{c} \right)^2 y_1 = 0 \quad (17)$$

$$\frac{d^2}{ds^2} y_2 + \left( \frac{\omega_\beta(\delta_2)}{c} \right)^2 y_2 = \frac{1}{m_e c^2 \gamma} e q \frac{1}{C} \mathcal{W}_\perp y_1,$$

where  $y_1$  and  $y_2$  are the transverse coordinates of macroparticles 1 and 2,  $\delta_1$  and  $\delta_2$  are the relative energy deviations ( $\Delta E/E$ ) of macroparticles from the design energy,  $\omega_\beta$  is the betatron oscillation frequency,  $q$  is the total bunch charge and



$\mathcal{W}_\perp$  the effective dipole wake. During the time period  $T_s/2 < s/c < T_s$  the equations of motion are again Eqn. (17) but with indices 1 and 2 exchanged. For the time interval  $T_s < s/c < 3T_s/2$  Eqn. (17) applies again, and so forth. The effective wake due to the head macroparticle can be estimated as the wake within the bunch at  $s = \sigma_z$ :

$$\mathcal{W}_\perp = W_1(\sigma_z). \quad (18)$$

The solution of the equations of motion (17) for zero chromaticity are:

$$y_n(s) = \tilde{y}_n(s) \exp(-i\Phi_{\beta_n}(s)), \quad n = 1, 2 \quad (19)$$

where  $\Phi_{\beta_n}(s)$  is the betatron phase and the amplitude functions  $\tilde{y}_n(s)$  are solutions of the equation [27]:

$$\begin{pmatrix} \tilde{y}_1 \\ \tilde{y}_2 \end{pmatrix}_{s=cT_s} = \begin{pmatrix} 1 - \Upsilon^2 & i\Upsilon \\ i\Upsilon & 1 \end{pmatrix} \begin{pmatrix} \tilde{y}_1 \\ \tilde{y}_2 \end{pmatrix}_{s=0}, \quad (20)$$

with the parameter  $\Upsilon$ , given by

$$\Upsilon = \frac{1}{m_e c^2 \gamma} e^2 N \frac{1}{C} \mathcal{W}_\perp \frac{\pi}{2} \frac{c^2}{\omega_\beta \omega_s}. \quad (21)$$

The transverse motion is stable if the trace of the matrix in Eqn. (20) is smaller than 2 or equivalently if

$$\Upsilon < 2. \quad (22)$$

Equations (21) and (22) are used to obtain an upper limit for the effective wake  $\mathcal{W}_\perp$  for the considered parameter sets. The results are summarized in Tab. 10.

|   | PETRA II |       | PETRA III |       | KEK-B LER |
|---|----------|-------|-----------|-------|-----------|
|   | 96 ns    | 10 ns | A         | B     | 573 mA    |
| Energy /GeV   | 7        | 7     | 6         | 6     | 3.5       |
| Circumference /m  | 2304     | 2304  | 2304      | 2304  | 3016      |
| $N /10^{10}$  | 5.0      | 4.1   | 0.5       | 24.0  | 3.0       |
| $Q_y$   | 23       | 23    | 31        | 31    | 43        |
| $Q_s$   | 0.06     | 0.06  | 0.05      | 0.05  | 0.01      |
| $\mathcal{W}_{\perp\text{limit}} / (\text{MV}/(\text{nC m}))$               | 26.3     | 32.1  | 253.6     | 5.3   | 5.5       |
| $(N \mathcal{W}_\perp)_{\text{limit}} / (10^{10} \text{ MV}/(\text{nC m}))$ | 131.5    | 131.5 | 126.6     | 126.6 | 16.3      |

Table 10: Limit for the wakefield

The PETRA III (variant A) design is by a factor of about 50 less sensitive to head-tail instabilities than the considered KEK-B LER variant with a bunch population of  $3.0 \cdot 10^{10}$ . The wakefield limits for the PETRA III (variant B) and

the considered KEK-B LER variant are almost the same. It is also interesting to translate the condition from Eqn. (22) into a limit on the product of the bunch population and the effective wakefield ( $N \mathcal{W}_\perp$ ). The results are shown in the last row of Tab. 10. It turns out that the KEK-B LER is by a factor of about 8 more sensitive to head-tail instabilities than the PETRA II/III rings which do not differ significantly with respect of this parameter  $(N \mathcal{W}_\perp)_{\text{limit}}$ .

### 4.3 Wakefields due to electron clouds

The wakefield of the electron cloud can be calculated from the electron cloud density according to Eqn. (14) and (16). The results are presented in Tab. 11, first under the assumption that the cloud density is equal to the average beam density (neutrality condition) and using the results for the center density from the computer simulations with the ECLOUD 2.3 code. The transverse wakefields

|  | PETRA II     |             | PETRA III    |              | KEK-B LER   |
|--|--------------|-------------|--------------|--------------|-------------|
|  | 96 ns        | 10 ns       | A            | B            | 573 mA      |
| Condition of neutrality  |              |             |              |              |             |
| volume density $\langle \rho_b \rangle / (10^{12} \text{ m}^{-3})$ | 0.31         | 2.47        | 1.66         | 1.66         | 1.8         |
| line charge density $\lambda_n / (10^5 \text{ m}^{-1})$            | 0.96         | 7.53        | 0.156        | 0.156        | 0.43        |
| $\omega_{bn} / (2\pi) / \text{kHz}$                                | 28.7         | 80.6        | 71.9         | 71.9         | 102.3       |
| $\hat{w}_{1n} / (\text{MV}/(\text{nC m}))$                         | 4.9          | 42.8        | 628.9        | 90.7         | 149.2       |
| $W_1(\sigma_z)_n / (\text{MV}/(\text{nC m}))$                      | 0.53         | 5.7         | 24.3         | 0.49         | 6.27        |
| $W_1(\sigma_z)_n / \mathcal{W}_{\perp \text{limit}}$               | 0.02         | 0.18        | 0.096        | 0.093        | 1.15        |
| Simulation   |              |             |              |              |             |
| center density $/ (10^{12} \text{ m}^{-3})$                        | 0.7          | 2.1         | 1.0          | 1.5          | 3.0         |
| line charge density $\lambda_c / (10^5 \text{ m}^{-1})$            | 2.14         | 6.41        | 0.094        | 0.141        | 0.72        |
| $\omega_b / (2\pi) / \text{kHz}$                                   | 42.9         | 74.3        | 55.8         | 68.4         | 131.9       |
| $\hat{w}_1 / (\text{MV}/(\text{nC m}))$                            | 11.0         | 36.5        | 379.1        | 82.1         | 248.4       |
| $W_1(\sigma_z) / (\text{MV}/(\text{nC m}))$                        | 1.2          | 4.9         | 14.7         | 0.45         | 10.4        |
| $W_1(\sigma_z) / \mathcal{W}_{\perp \text{limit}}$                 | <b>0.045</b> | <b>0.15</b> | <b>0.058</b> | <b>0.085</b> | <b>1.91</b> |

Table 11: Effective transverse wakefield due to the electron cloud. The results are based on estimates from the condition of neutrality and on the center density obtained from computer simulations.  $W_1(\sigma_z)$  is the dipole wakepotential at the position  $s = \sigma_z$  in the tail of the bunch.

$W_1(\sigma_z)$  due to the electron cloud have been compared with the previously calculated limit from the instability threshold. The wakefield is well below ( $< 0.2$ ) the instability threshold for all considered parameter sets for PETRA II/III. For the considered KEK-B LER parameters a head-tail instability is expected since the wakefield due to the electron cloud is above the limit. This is in agreement with the experimental observations of a beam blow-up [2]. The condition of neutrality seems to be in most cases a very useful estimate of the electron cloud density.

The results of the simulation PETRA III with a photoelectron yield of  $Y = 1.0$  is not included in Tab. 11. The center density for that case is  $3.5 \cdot 10^{12} \text{ m}^{-3}$ , from which an effective transverse wake of  $W_1(\sigma_z) = 51.4 \text{ MV}/(\text{nC m})$  is obtained. This is still well below the instability threshold ( $W_1(\sigma_z)/\mathcal{W}_{\perp\text{limit}} = 0.2$ ).

## 5 Summary and conclusion

It is planned to rebuild the PETRA ring, presently used as a preaccelerator for the HERA rings, into a third generation synchrotron light source, called PETRA III. Since it is considered to use a positron beam for PETRA III the build-up of electron clouds was investigated and presented in this paper. In section 2 the parameters of the present PETRA ring and the planned PETRA III storage ring needed for simulations, namely beam and optics parameters as well as the vacuum chamber dimensions, have been introduced. The production of photoelectrons has been estimated from the material properties of Aluminum. The parameters which are important for the production of secondary electrons have been discussed, too.

The computer code ELOUD 2.3 has been used to simulate the electron cloud build-up in PETRA II & III for different parameter sets. Furthermore the KEK B-factory low energy ring has also been simulated since strong effects from electron clouds have been experimentally observed at that storage ring. No instabilities due to electron clouds have been observed for the PETRA II ring, a result which has also been found in the simulations. The agreement of the simulations with experiments for existing rings gives confidence in the predictions for PETRA III.

An effective transverse wake potential at the position  $\sigma_z$  within the bunch has been calculated from the simulated density of the electron cloud in the center of the beam using a broad band resonator model. The wake potential has been compared to a wake limit for a head-tail instability obtained from a two particle model. It has been found that no single bunch instability due to electron clouds is expected for the planned PETRA III synchrotron light source. The main results from the simulation and predictions for the transverse wake are:

|   | PETRA II<br>96 ns | PETRA III<br>A   B |       | KEK-B<br>LER 573 mA |
|---|-------------------|--------------------|-------|---------------------|
| Cloud Population / $10^{10}$ / m                | 0.46              | 0.32               | 2.2   | 2.9                 |
| Average density / $(10^{12} \text{ m}^{-3})$    | 0.83              | 1.3                | 8.7   | 4.2                 |
| Center density / $(10^{12} \text{ m}^{-3})$     | 0.7               | 1.0                | 1.5   | 3.0                 |
| $W_1(\sigma_z) / (\text{MV}/(\text{nC m}))$     | 1.2               | 14.7               | 0.45  | 10.4                |
| $W_1(\sigma_z)/\mathcal{W}_{\perp\text{limit}}$ | 0.045             | 0.058              | 0.085 | 1.91                |

A field free region has always been used in the simulation. The synchrotron radiation from a bending magnet with a bending radius of about 192 m has been used for the PETRA II/III calculations. In the new section of the planned

PETRA III ring, dipole magnets with a bending radius of about 23 m will be used. Additional damping wiggler sections will be installed in PETRA III which will radiate synchrotron radiation with a spectrum different from the dipole radiation spectrum used in the simulation. This will most likely have no significant impact on the single bunch instability of the beam since these sections are short compared to the total circumference of the ring. Nevertheless the electron cloud density may be locally higher than predicted under the assumptions made for the simulations. This can have an impact on the local vacuum pressure and should be studied in connection with the design of the vacuum system.

## Acknowledgment

I would like to thank K. Balewski and W. Brefeld for many discussion on PETRA III and their interest in the subject of electron clouds. Thanks go also to F. Zimmermann for useful comments and his help and support with the E-CLOUD computer code which has been used for all simulations shown in this report. I thank M. Schwartz and W. Giesske for providing the vacuum chamber drawings and M. Lomperski for carefully reading the manuscript.

## References

- [1] K. Balewski, W. Brefeld, Y. Li, *PETRA-III - eine dedizierte Synchrotronstrahlungsquelle*, Vorstudie, 2001, unpublished
- [2] H. Fukuma, *Electron cloud effects at KEKB*, Proc. of E-CLOUD'02: Mini-Workshop on Electron-Cloud Simulations for Proton and Positron Beams, CERN, Geneva, April 2002.
- [3] Kulikov et al., *The electron cloud instability at PEP II* Proceedings PAC 2001, Particle Accelerator Conference, Chicago, June, 2001
- [4] M. Izawa, Y. Sato, T. Toyomasu, *The vertical instability in a positron bunched beam*, Phys. Rev. Lett. **74** (1995) 5044
- [5] K. Ohmi, *Beam and photoelectron interactions in positron storage rings*, Phys. Rev. Lett. **75** (1995) 1526
- [6] G. Budker, G. Dimov, V. Dudnikov, *Experiments on production of intense proton beam by charge exchange injection method*; Proceedings of the International Symposium on Electron and Positron Storage Rings, Saclay, France, VIII, 6.1 (1966)
- [7] O. Grobner, *Bunch induced multipactoring*, Proceedings of 10th Int. Conf. on High Energy Acc., Protvino (1977) 277
- [8] F. Zimmermann, *The Electron Cloud Instability: Summary of Measurements and Understanding*, Proc. of IEEE Particle Accelerator Conference (PAC 2001), Chicago, 2001
- [9] F. Zimmermann et al., *Present understanding of electron cloud effects in the Large Hadron Collider*, Proceedings PAC 2003, Particle Accelerator Conference, Portland, May 12-16, 2003
- [10] M.A. Furman, *Formation and Dissipation of the Electron Cloud*, Proceedings PAC 2003, Particle Accelerator Conference, Portland, May 12-16, 2003

- [11] K.C. Harkay, R.A. Rosenberg, *Properties of the electron cloud in a high-energy positron and electron storage ring*, Phys. Rev. ST Accel. Beams **6**, 034402 (2003)
- [12] F. Zimmermann, G. Rumolo, *Electron-Cloud Simulations: Build-Up and Related Effects*, Proc. of ELOUD'02: Mini-Workshop on Electron-Cloud Simulations for Proton and Positron Beams, CERN, Geneva, April 2002.
- [13] K. Balewski, W. Brefeld, *PETRA optics*, private communication
- [14] J. Kouptsidis, G.A. Mathewson, *Reduction of the photoelectron induced re-sorption in the PETRA vacuum system by in situ argon glow discharge*, DESY internal report, DESY76/49, Sept. 1976
- [15] M. Sands, *The physics of electron storage rings*, SLAC-121, 1970
- [16] J. Schwinger, *On the classical radiation of accelerated electrons*, Phys. Rev. **75**, 1912-1925 (1949)
- [17] O. Gröbner, et al., *Neutral gas desorption and photoelectric emission from aluminum alloy vacuum chambers exposed to synchrotron radiation*, J. Vac. Sci. Technol. A **7** (2) Mar/Apr 1988
- [18] F. Zimmermann, *An estimate of gas resorption in the damping rings of the Next Linear Collider*, NIM A **398** (1997), 131-138
- [19] K. Ohmi, *Electron cloud effect in the damping ring of Japan Linear Collider*, Proc. of ELOUD'02: Mini-Workshop on Electron-Cloud Simulations for Proton and Positron Beams, CERN, Geneva, April 2002.
- [20] N. Hilleret et al., *Secondary electron emission data for the simulation of electron cloud*, Proc. of ELOUD'02: Mini-Workshop on Electron-Cloud Simulations for Proton and Positron Beams, CERN, Geneva, April 2002.
- [21] M. A. Furman, *The electron-cloud effect in the arcs of the LHC*, CERN-LHC-PROJECT-REPORT-180, May 1998
- [22] N. Hilleret et al., *The secondary electron yield of technical materials and its variation with surface treatments*, 7th European Particle Accelerator Conference, EPAC 2000, Vienna, Austria , 26 - 30 Jun 2000
- [23] N. Hilleret, *An empirical fit to the true secondary electron energy distribution*, unpublished, CERN, 2001
- [24] *KEK B-Factory Design Report*, KEK Report 95-7, 1995

- [25] K. Ohmi, F. Zimmermann, *Study of head-tail effect caused by electron cloud*, 7th European Particle Accelerator Conference, EPAC 2000, Vienna, Austria, 26 - 30 Jun 2000
- [26] K. Ohmi, F. Zimmermann, E. Perevedentsev, *Wake-Field And Fast Head - Tail Instability Caused By An Electron Cloud* , Phys. Rev. E **65** (2002) 016502.
- [27] R. D. Kohaupt, *Simplified presentation of head tail turbulence*, Internal Report, DESY M-80/19, Oct. 1980